Biointerface Research in Applied Chemistry
Open-Access Journal (ISSN: 2069-5837)

Article
Volume 13, Issue 3, 2023, 236
https://doi.org/10.33263/BRIAC133.236

Different Methods for Preparation of Hydroxyapatite Nanostructures

Nehal Salahuddin [1,*], Ebtisam Mohamed Ibrahim [2], Maged El-Kemary [3,*]

[1] Department of Chemistry, Faculty of Science, Tanta University, 31527, Tanta, Egypt, nehal.attaf@science.tanta.edu.eg, salahuddin.nehal@yahoo.com (N.S.);
[2] Department of Chemistry, Faculty of Science, Nanotechnology center, Kafr Elsheikh University, 33516 Kafr Elsheikh, Egypt
[3] Institute of Nanoscience & Nanotechnology, Kafr Elsheikh University, 33516 Kafr Elsheikh, Egypt
* Correspondence: nehal.attaf@science.tanta.edu.eg (N.S.); ebtisam_mi@yahoo.com (E.M.I); elkemary@nano.kfs.edu.eg (M.E);

Scopus Author ID 6602179027
Received: 29.12.2022; Accepted: 24.01.2022; Published: 6.06.2022

Abstract: Hydroxyapatite could be utilized as a bioceramic due to its osteoconductivity and bioactivity. The shape of HAp nanoparticles influences their properties, such as bioactivity and surface area. Nano-sized HAp particles with different morphologies were synthesized using a variety of preparation processes such as solvothermal, microwave-solvothermal, precipitation, and hydrothermal-precipitation process. The effect of preparation methods on particle morphology was studied. The X-ray diffraction (XRD), Fourier-transform infrared spectroscopy (FTIR), transmission electron microscopy (TEM), scanning electron microscopy (SEM), and Zeta potential (ZP), were used to validate the composition and structure of the as-formulated HAp nanostructures. A single phase of HAp was obtained using various methods of preparation. According to the TEM analysis of the powders, both the solvothermal and the hydrothermal treatment samples were very diffuse and consisted of fairly homogeneous HAp nanorods.

Keywords: Hydroxyapatite; Nanorods; Hydrothermal; Precipitation; Solvothermal; Microwave

1. Introduction

Calcium phosphate has been extensively studied for potential biomedical uses because of its exceptional biocompatibility [1-3]. Among other calcium phosphates, hydroxyapatite $Ca_{10}(PO_4)_6(OH)_2$ (HAp) has sparked a lot of interest in biomedical fields owing to its outstanding features such as nontoxicity, bioactivity, outstanding biocompatibility, noninflammatory and nonimmunogenicity inorganic material, biodegradability, osteoconductivity and under physiological conditions, hydroxyapatite is the most stable calcium phosphate crystalline form. These characteristics are due to HAp's chemical composition, which mimics the inorganic components of human teeth and bone [1]. Synthetic HAp can be dissolved at a low pH value to form non-toxic Ca^{2+} ions and PO_4^{3-} ions in an aqueous solution. As a result, because inflammatory tissues and tumors have lower pH values than normal tissues and blood, HAp nanostructured materials can be developed and utilized as a pH-triggered medication delivery system to regulate medication liberate [4,5].

Furthermore, HAp has two distinct binding sites on its surface (negatively charged P sites and positively charged C sites) [6]. Because of their great affinity, HAp nanoparticles have been investigated as one of the most auspicious delivery vehicles for diverse biomolecules such as proteins, hormones, and gene transfection [7-10]. Numerous HAp nanostructured materials with various shapes have been created using various procedures to satisfy the requirements of biomedical purposes. The preparation procedures significantly impact the physicochemical properties, chemical composition, structure, morphology, size, and crystallinity of synthetic HAp materials [11]. As a result, applications of the HAp nanoscale could be improved by controlling the morphology of HAp nanostructure, such as a rod-like, plate-like, needle-like, or spherical shape. Therefore, in recent years, great research attempts have been dedicated to improving HAp powders' morphology [12]. Recent interest has peaked in producing surface-functionalized nanoscale materials with relevant characteristics for medication delivery applications. It is commonly acknowledged that the surface modification of nanomaterials can provide a variety of important benefits as a result of the nanoparticles' combined capabilities and the substance in which they are coated [13-16]. Surface functionalization of HAp could modify their behavior in physiological solutions by regulating their contact with tissue in vivo. Moreover, surface functionalization can be used to create stimulus-responsive nanocarriers that can regulate medication diffusion in response to external and internal triggers such as temperature and pH [17-20]. Various chemical modifiers have been used to modify the morphology, including cetyltrimethylammonium bromide (CTAB), ethylene glycol, polyvinyl alcohol, and ethylene diamine tetra-acetic acid (EDTA), hydroxyl, amine, carboxyl, thiol, and phosphate [12]. Citric acid has been frequently employed for surface functionalization of nanomaterials among several functionalities. HAp nanorods (HAp NRs) have been widely studied for medication delivery and bio-imaging applications, among other morphologies [21-23], because of their small dimensions, high affinity for various substances, and good crystallinity. This study aimed to create various grain size morphologies of HAp nanostructures using different preparation methods such as solvothermal, microwave-solvothermal, precipitation, and hydrothermal-precipitation.

2. Materials and Methods

2.1. Materials.

Dipotassium hydrogen phosphate anhydrous (K_2HPO_4, 99% AppliChem Panreac, ITW Companies), calcium chloride anhydrous ($CaCl_2$, 99% AppliChem Panreac, ITW Companies), ethylene diamine (EDA $C_2H_8N_2$; 99%, Merck), ethylene glycol (EG 99%, Merck, Germany), sodium hydroxide pellets (NaOH, 99% Merck, Germany), and ethanol (C_2H_5OH, 95%, Pio chem, Egypt) were used as received.

2.2 Methods.

2.2.1. Solvothermal and microwave-solvothermal approaches.

For the preparation of HAp nanorods, 0.00294 moles of $CaCl_2$ was dissolved in 25 mL binary solvent of ethylene glycol (EG), and double-distilled H_2O with volume ratios of 1:1 and 0.00175 mole of $K_2H\ PO_4$ was dissolved in another 25 mL binary solvent of EG and double-distilled H_2O (1:1 v/v). Then, drop by drop, the $CaCl_2$ solution was poured into the K_2HPO_4 solution. Subsequently, 50 mL ethylene diamine was added to the above-mixed suspension at

1.0 mL/ min. The pH of the suspension was attuned to 11 using NaOH solution (1M); then, 70 mL of the obtained suspension was transferred into a stainless-steel autoclave with *a* 100 mL Teflon vessel and subsequently transferred into an oven heated to 200 ºC and preserved at 200 °C for 12 h and 24 h to produce HAp NRs_{sol12} and HAp NRs_{sol24} respectively. In addition, 25 ml was transferred to a 50 mL quartz vessel, hosted in a safety shield, and put inside the cavity of a microwave reactor (Milestone Microwave Synthesis Labstation Model Start Synth) heated to 200 °C and preserved at this temperature for 10 min and 30 min to afford HAp NRs_{MW10} and HAp NRs_{MW30} respectively. Following cooling to ambient temperature, the obtained precipitate was centrifuged, rinsed several times with double-distilled H_2O and ethanol, and then dried for 24 hours at 70 °C for further structure determination.

2.2.2 Precipitation approach.

A modified co-precipitation method [17] was used to produce citrate-functionalized hydroxyapatite nanorods. Concisely, solution a was obtained by dissolving 1.5 g citric acid and 14.765 mmoles of anhydrous calcium chloride in 50 mL double-distilled H_2O and adjusting the pH with NaOH solution (1M) to 11.0, and solution b was made by dissolving 8.84 mmoles of K_2HPO_4 in 30 ml of double-distilled H_2O and keeping the pH at 11.0 using 1 M sodium hydroxide solution. Then, with vigorous stirring, solution b was added drop by drop to solution a, at a rate of one ml per min. The stirring was prolonged for another two hours after the precipitation was completed. Throughout the experiment, the pH of the suspension was kept at 11. The final suspension was stirred for 24 hours. The precipitate (CF-HAp NRs_{ppt}) was centrifuged at 6000 rpm for 5 minutes, then rinsed multiple times with double-distilled H_2O and ethanol before being dried in an oven at 70 ºC for twenty four hours. In the lack of citric acid, the same technique was used to create hydroxyapatite nanorods (HAp NRs_{ppt}).

2.2.3 Hydrothermal - precipitation approach.

A hydrothermal precipitation approach was used to produce uniform Citrate-functionalized HAp nanorods. In brief, two solutions were ready: Solution a was set by dissolving 1.2 g citric acid and 0.01181 moles of anhydrous calcium chloride in 40 ml double-distilled H_2O, and the pH of the solution was preserved at 11.0 by adding 1 M sodium hydroxide solution, and solution b were ready by dissolving 0.007 moles of K_2HPO_4 in 24 ml double-distilled H_2O, with keeping the pH of the solution at 11.0 by adding 1 M sodium hydroxide solution. Then one ml per min of solution b was put in solution a drop by drop with stirring. The stirring was prolonged for another two hours after the precipitation was completed. Throughout the experiment, the pH of the suspension was preserved at 11.0. The final suspension was placed into a stainless-steel autoclave with a 100 mL Teflon vessel and subsequently transferred into an oven heated to 200 ºC and preserved at 200 ºC for twelve hours. The product (CF-HAp NRs_{hyd}) was separated after cooling to room temperature by centrifugation at 6000 rpm for ten minutes, washing three times with double-distilled H_2O and ethanol. Finally, the precipitate (CF-HAp NRs_{hyd}) was maintained for drying in an oven at 70 ºC for twenty-four hours.

2.3. Characterization.

On an FTIR -4100 spectrometer JASCO, FTIR spectra were assessed using KBr disks at a frequency scale from 4000 to 400 cm^{-1}. An X-ray diffractometer, XRD-6000, Shimadzu,

Japan with Cu-kα radiation (λ =1.5412 Å), 40 Kv, 30 mA) in the 2θ range of 10-80° with 2°/min scanning rate was used to determine the crystallinity and phases of the HAP nanostructures. The morphological features of a high-resolution transmission electron microscope (SEM-EDS, JSM-6360 LA, JEOL, Japan) and a high-resolution transmission electron microscope (HRTEM, JEM-2100, JEOL) are the morphological features of the nanostructures, and the Ca/P ratio of samples were determined. At 30 °C, the samples' Zeta potential was evaluated using Zetasizer (ZetaPALS zeta potential analyzer, Brookhaven Instruments Co., USA); the samples were diluted with deionized water.

3. Results and Discussion

3.1. Powder X-ray diffraction analysis.

Figure 1 reveals the XRD patterns of the HAp nanostructures. It is obvious that the distinctive peaks detected for HAp nanostructures are understood to be in good agreement with those of the Joint Committee for Powder Diffraction Standards (JCPDS) data (04-008-4761) for HAp. The XRD patterns show that all samples synthesized by various procedures have similar XRD patterns, which can be indexed to a single phase of hydroxyapatite (HAp). The crystalline phase of the samples is evidenced by the significant peaks at 25.9° (002), 28.1° (102), 29° (210), 31.8° (211), 32.2° (112), 32.9° (300), 34° (202), 39.8° (310), 41.8° (302), 43.5° (123), 44.9° (400), 46.7° (222), 48.1° (312), 49.3° (213) and 53° (004). The absence of diffraction peaks related to contaminants in the XRD patterns indicates that the products generated are of high purity [24].

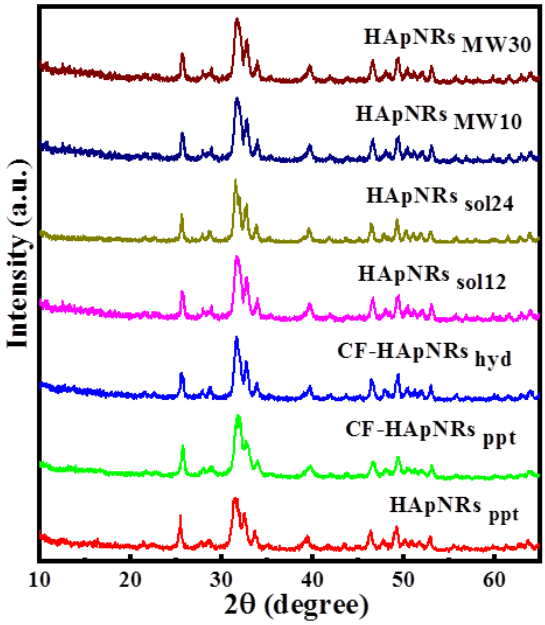

Figure 1. XRD patterns of HAp nanorods prepared via different methods.

3.2. Fourier- transform infrared spectroscopy analysis

The compositions of the samples prepared by different methods were further investigated by FTIR, and the spectra are shown in Figure 2. It can be observed that the apatite hydroxyl bond and phosphate radicals are responsible for the majority of the typical adsorption peaks in the spectrum, indicating that HAp was successfully synthesized. The absorption band at 3000-3550 cm^{-1} could be attributed to OH stretching [24,25]. The vibration mode of carbonate ions could be accountable for the peaks at 1417 and 874 cm^{-1}, which were probably

wrapped up from the atmosphere through the sample formulation under alkaline circumstances [24,25]. The bands at 1039 and 1097 cm^{-1} are caused by the triply degenerate ν_3 asymmetric P-O stretching mode. The non-degenerate P-O symmetric stretching ν_1 mode was responsible for the peak detected at 963 cm^{-1}. The band at 474 cm^{-1} could be dispensed to the doubly degenerate ν_2 bending of O-P-O mode. The peak at 568 and 603 cm^{-1} were attributed to the triply degenerate ν_4 bending of O-P-O mode. The $-CH_2$, $-CH_3$, and C=O stretching vibrations are ascribed to the absorption peaks at 2926, 2857, and 1639 cm^{-1}, respectively [26]. Moreover, the C=O asymmetric and symmetric stretching of the carboxyl group (COO^-) were detected at 1560 and 1420 cm^{-1}, respectively, demonstrating that the citric acid in CF-HAp NRs_{ppt} and CF-HAp NRs_{hyd} has been well modified [21], while these peaks were not present in unfunctionalized HAp.

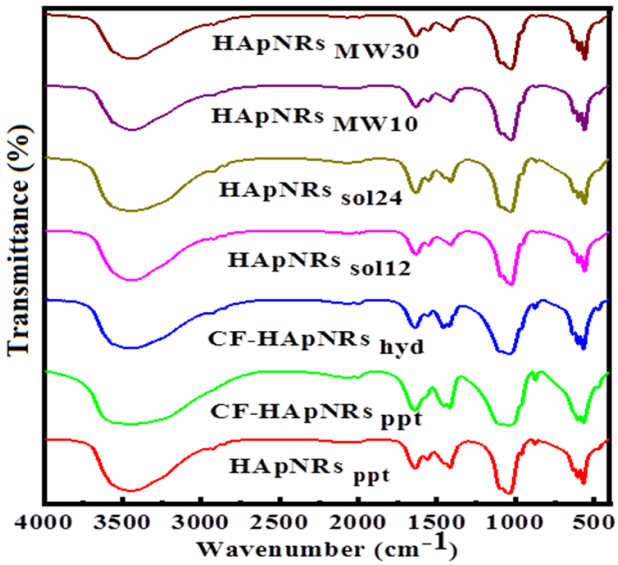

Figure 2. FTIR spectra of HAp nanorods prepared via different methods.

3.3. Transmission Electron Microscopy analysis.

Transmission electron microscopy (TEM) was used to assess the effect of different preparation procedures on the morphology of the HAp nanostructures. The TEM micrographs in Figure 3a, b, demonstrate that the sample prepared by the solvothermal approach at 200 °C for 12 h comprised well-defined, uniform HAp nanorods with diameters of about 16.5 nm and lengths of 58 nm (Figure S1a,b). When the reaction time increased to 24 h Figure 3c, d, the sample also comprised of homogenous HAp nanorods with average diameter of 16.88 nm and average length of 55.7 nm (Figure S1c,d). Figure 3e, f, shows the TEM micrographs of the microwave-assisted solvothermal samples at different reaction times. The TEM micrographs show that the HAp nanostructures prepared at 200 °C for 10 min possess rod-like shapes with an average diameter of 8.9 nm and an average length of 42.4 nm (Figure S2a,b), while the sample prepared at 200 °C for 30 min comprised of HAp nanorods of the average diameter of 7.6 nm and the average length of 55 nm (Figure S2c,d). Figure 4, presents TEM micrograph of all the HAp nanostructures prepared by precipitation and hydrothermal-precipitation approaches. TEM micrographs show that all HAp nanostructures possess rod-like morphology. Comparing HAp prepared by precipitation method with and without citric acid with HAp prepared by the hydrothermal method in the presence of citric acid, it was found that the sample synthesized without the hydrothermal treatment comprises nanorods that were highly aggregated.

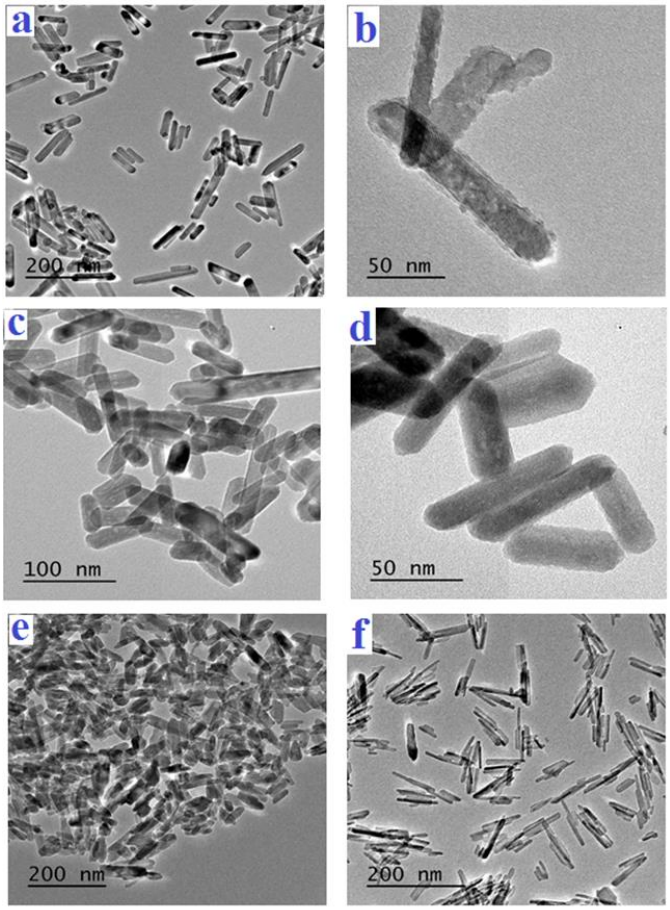

Figure 3. TEM micrographs at different magnification of (a,b) HAp NRs_{sol12}, (c,d) HAp NRs_{sol24} , (e) HAp NRs_{MW10} and (f) HAp NRs_{MW30}.

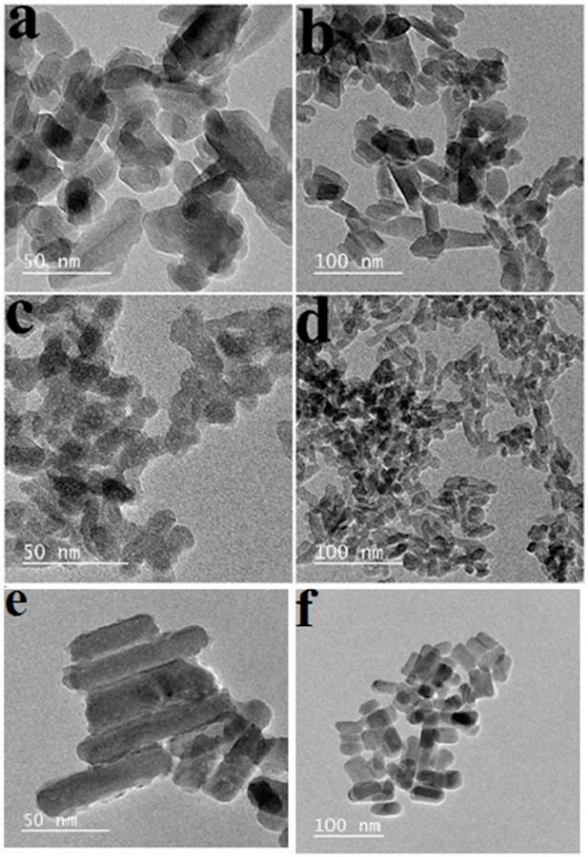

Figure 4. TEM micrographs at different magnification of (a,b) HAp NRs_{ppt}, (c,d) CF-HAp NRs_{ppt} and (e,f) CF-HAp NRs_{hyd}.

On the other hand, the size and morphology of the sample synthesized by the hydrothermal treatment were well disseminated and constituted of reasonably homogenous HAp nanorods with an average length of 65.24 nm and average diameter of 15.75 nm (Figure S3e,f) [10, 27]. In addition, the HAp nanostructure powders were subjected to compositional analysis to determine the Ca/P molar ratio (Figure 5). According to EDX analysis, the synthesized HAp nanostructures have a Ca/P ratio of 1.66, which is near to apatite's theoretical value (1.67) [28].

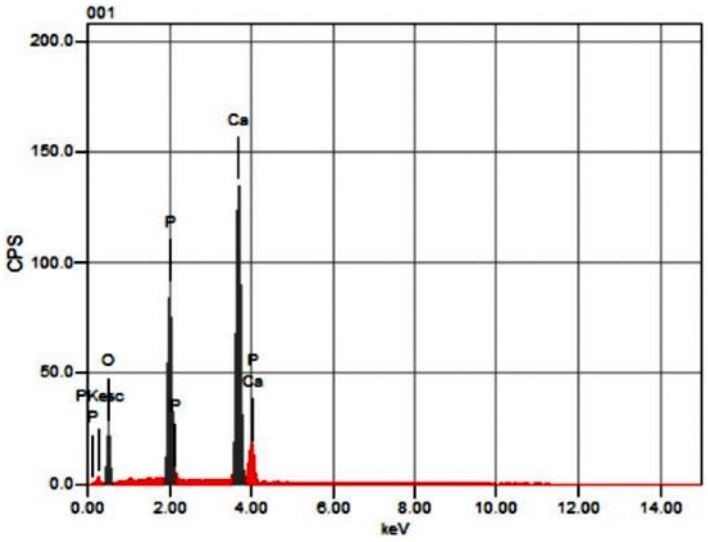

Figure 5. EDX spectrum of hydroxyapatite nanorods.

3.4. Zeta-potential measurements.

Figure 6 reveals the zeta potential of the samples. As revealed in Figure 6, the zeta potential of HAp NRs prepared by microwave-solvothermal and solvothermal approaches were more positive than HAp NRs prepared by precipitation and hydrothermal-precipitation method in the occurrence of citric acid.

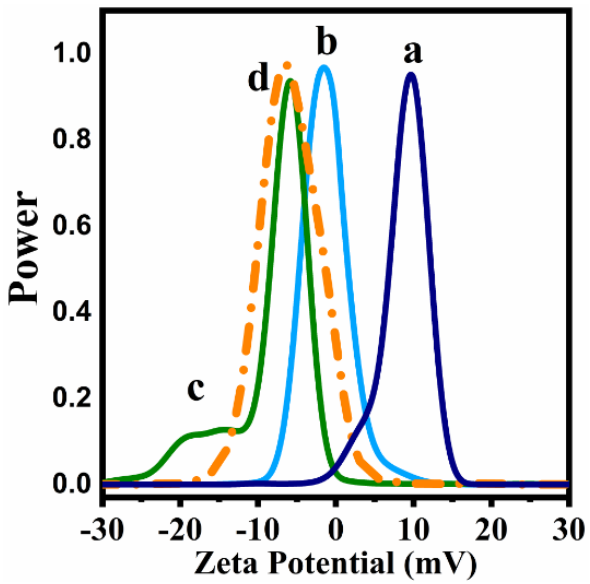

Figure 6. Zeta potential of (a) HAP NRs_{sol24}, (b) HAp NRs_{ppt}, (c) CF-HAp NRs_{ppt}, and (d) CF-HAp NRs_{hyd}.

4. Conclusions

This study studied the impact of various preparation methods on particle morphology using TEM. The sample formulated without the solvothermal, and the hydrothermal treatment

comprises highly aggregated nanorods. However, uniform, well-defined hydroxyapatite nanorods have been successfully synthesized using solvothermal and hydrothermal-precipitation methods. The formation of hydroxyapatite nanostructures was established using X-ray diffraction (XRD) and Fourier transform infrared (FTIR) spectroscopy. According to EDX analysis, the synthesized HAp nanostructures have a Ca/P ratio of 1.66, which is near apatite's theoretical value (1.67). The zeta potential of nanorods ranged from 10 to -10 mV depending on the preparation method and functionalization of nanostructures.

Funding

This research received no external funding.

Acknowledgments

This research has no acknowledgments.

Conflicts of Interest

The authors declare no conflict of interest.

References

1. Qi, C.; Zhu, Y-J.; Ding, G-J.; Wu, J.; Chen, F. Solvothermal synthesis of hydroxyapatite nanostructures with various morphologies using adenosine5'-monophosphate sodium salt as an organic phosphorus source. *RSC Adv* **2015**, *5*, 3792-3798, https://doi.org/10.1039/C4RA13151G.
2. Du, M.; Chen, J.; Liu, K.; Xing, H.; Song, C. Recent advances in biomedical engineering of nano-hydroxyapatite including dentistry, cancer treatment and bone repair. *Compos. B. Eng.* **2021**, *215*, 108790, https://doi.org/10.1016/j.compositesb.2021.108790.
3. Bhandari, N. L.; Bista, S.; Gautam, T. R.; Bist, K.; Bhandari, G.; Subedi, S.; Dhakal, K. N.; An overview of synthesis based biomedical applications of hydroxyapatite nanomaterials. *J. Nepal Chem. Soc.* **2021**, *42*, 64-74, https://doi.org/10.3126/jncs.v42i1.35333.
4. Fan, Q.; Fan, F.; Xu, W.; Zhang, H.; Liu, N. The structural and surface properties of Al-doped hydroxyapatite (Ca5(PO4)3OH) nanorods and their applications foe pH-induced drug delivery. *J. Alloys Comp.* **2021**, *879*, 160414, https://doi.org/10.1016/j.jallcom.2021.160414.
5. Zhou, L.; Zhang, Y.; Zeng, D.; Shu, T.; Wang, S. Dual-responsive mesoporous poly-N-isopropylacrylamide-hydroxyapatite composite microspheres for controlled anticancer drug delivery. *J. Sol-Gel. Sci. Technol.* **2021**, *97*, 600-609, https://doi.org/10.1007/s10971-020-05460-3.
6. Shi, H.; Zhou, Z.; Li, W.; Fan, Y.; Li, Z.; Wei, J. Hydroxyapatite based materials for bone tissue engineering: A brief and comprehensive introduction. *Crystals* **2021**, *11*, 149, https://doi.org/10.3390/cryst11020149.
7. Kadu, K.; Kowshik, M.; Ramanan, S. R. Does the nanoparticle morphology influence interaction with protein: A case study with hydroxyapatite nanoparticles. *Mater. Today Commun.* **2021**, *26*, 102172, https://doi.org/10.1016/j.mtcomm.2021.102172.
8. Halim, N. A. A.; Hussein, M. Z.; Kandar, M. K. Nanomaterials-Upconverted hydroxyapatite for bone tissue engineering and a platform for drug delivery. *Int. J. Nanomedicine*. **2021**, *16*, 6477-6496, https://doi.org/10.2147/IJN.S298936.
9. Panda, S.; Biswas, C. K.; Paul, S. A comprehensive review on the preparation and application of calcium hydroxyapatite: A special focus on atomic doping methods for bone tissue engineering. *Ceram. Int.* **2021**, *47*, 28122-28144, https://doi.org/10.1016/j.ceramint.2021.07.100.
10. Song, T.; Zhao, F.; Wang, Y.; Li, D.; Lei, N.; Li, X.; Xiao, Y.; Zhang, X. Constructing a biomimetic nanocomposite with the in situ deposition of spherical hydroxyapatite nanoparticles to induce bone regeneration. *J. Mater. Chem. B.* **2021**, *9*, 2469-2482, https://doi.org/10.1039/D0TB02648D.
11. Biedrzycka, A.; Skwarek, E.; Hanna, U.M. Hydroxyapatite with magnetic core: Synthesis methods, properties, adsorption and medical applications. *Adv. Colloid Interface Sci*. **2021**, *291*, 102401, https://doi.org/10.1016/j.cis.2021.102401.

12. Yousefi, K.; Zebarjad, S, M.; Khaki, J, V. Comparison of polyethylene glycol effect on hydroxyapatite morphology produced into different methods: sol-gel and precipitation. J. Sol-Gel. Sci. Technol. 2015, 76, 592-598, DOI is: 10.1007/s10971-015-3809-y
13. Chang, L.; Huang, S.; Zhao, X.; Hu, Y.; Ren, X.; Mei, X.; Chen, Z. Preparation of ROS active and photothermal responsive hydroxyapatite nanoplatforms for anticancer therapy. *Mater. Sci. Eng. C* **2021**, *125*, 112098, https://doi.org/10.1016/j.msec.2021.112098.
14. Li, D.; Huang, X.; Wu, Y.; Li, J.; Cheng, W.; He, J.; Tian, H.; Huang, Y. Preparation of pH-responsive mesoporous hydroxyapatite nanoparticles for intracellular controlled release of an anticancer drug. *Biomater. Sci* **2016**, *4*, 272–280, https://doi.org/10.1039/C5BM00228A.
15. Li, J.; Liu, M.; Qiu, Y.; Gan, Y.; Jiang, H.; Liu, B.; Wei, H.; Ma, N. Urchin-like hydroxyapatite/graphene hollow microspheres as pH-responsive bone drug carriers. *Langmuir* **2021**, *37*, 4137-4146, https://doi.org/10.1021/acs.langmuir.0c03640.
16. Liang, Y. J.; Yang, I.; Lin, Y. W.; Lin, J. N.; Wu, C. C.; Chiang, C. Y.; Lai, K. H.; Lin, F. H. Curcumin-loaded hydrophobic surface-modified hydroxyapatite as an antioxidant for sarcopenia prevention. *Antioxidants* **2021**, *10*, 616, https://doi.org/10.3390/antiox10040616.
17. Verma, G.; Barick, K. C.; Shetake, N. G.; Pandeyb, B. N.; Hassana, P. A. Citrate-functionalized hydroxyapatite nanoparticles for pH-responsive drug delivery. *RSC Adv* **2016**, *6*, 77968-77976, https://doi.org/10.1039/C6RA10659E.
18. Verma, G.; Shetekeb, N. G.; Baricka, K. C.; Pandeyb, B. N.; Hassana, P. A.; Priyadarsin, K. I. Covalent immobilization of doxorubicin in glycine functionalized hydroxyapatite nanoparticles for pH-responsive release. *New J. Chem* **2018**, *42*, 6283-6292, https://doi.org/10.1039/C7NJ04706A.
19. Mondal, S.; Dorozhkin, S. V.; Pal, U. Recent progress on fabrication and drug delivery applications of nanostructured hydroxyapatite. *WIREs Nanomed Nanobiotechnol* **2018**, *10*, e1504, https://doi.org/10.1002/wnan.1504.
20. Presanna, A. P. S.; Venkatasubbu, G. D. Sustained releases of amoxicillin from hydroxyapatite nanocomposite for bone infections. *Prog Biomater* **2018**, *7*, 289-296, https://doi.org/10.1007/s40204-018-0103-4.
21. Lee, W. H.; Loo, C. Y.; Rohanizadeh, R. Functionalizing the surface of hydroxyapatite drug carrier with carboxylic acid groups to modulate the loading and release of curcumin nanoparticles. *Mater. Sci. Eng. C* **2019**, *99*, 929-939, https://doi.org/10.1016/j.msec.2019.02.030.
22. Zhang, C.; Shan, S.; Hu, T.; Wang, G.; Zhi, Y.; Su, H.; Jiang, L.; Ni, Y. Recent progress on biomedical applications of functionalized hollow hydroxyapatite microspheres. *Ceram. Int* **2021**, *47*, 13552-13571, https://doi.org/10.1016/j.ceramint.2021.01.214.
23. Jiang, Y.; Yuan, Z.; Huang, J. Substituted hydroxyapatite: a recent development. *Mater Technol* **2020**, *35*, 785-796, https://doi.org/10.1080/10667857.2019.1664096.
24. An, L.; Li, W.; Xu, Y.; Zeng, D.; Cheng, Y.; Wang, G. Controlled additive-free hydrothermal synthesis and characterization of uniform hydroxyapatite nanobelts. *Ceram. Int* **2016**, *42*, 3104-3112, https://doi.org/10.1016/j.ceramint.2015.10.099.
25. Chandra, V. S.; Elayaraja. K.; Arul, K. T.; Ferraris, S.; Spriano, S. Ferraris, M.; Asokan, K.; Kalkura, S. N. Synthesis of magnetic hydroxyapatite by hydrothermal-microwave technique: Dielectric, protein adsorption, blood compatibility and drug release studies. *Ceram. Int* **2015**, *41*, 13153-13163, https://doi.org/10.1016/j.ceramint.2015.07.088.
26. Qi, C.; Tang, Q-L.; Zhu, Y-J, Zhao, X-Y.; Chen, F. Microwave-assisted hydrothermal rapid synthesis of hydroxyapatite nanowires using adenosine 5-triphosphate disodium salt. *Mater. Lett* **2012**, *85*, 71-73, https://doi.org/10.1016/j.matlet.2012.06.106.
27. Ji, Y.; Wang, A.; Wu, G.; Yin, H.; Liu, S.; Chen, B.; Liu, F.; Li, X. Synthesis of different sized and porous hydroxyapatite nanorods without organic modifiers and their 5-fluorouracil release performance. *Mater. Sci. Eng. C* **2015**, *57*, 14-23, https://doi.org/10.1016/j.msec.2015.07.008.
28. Zhan, J. H.; Tseng, Y. H.; Chan, J. C. C.; Mou, C. Y. Biomimetic formation of hydroxyapatite nanorods by a single-crystal-to-single crystal transformation. *Adv. Funct. Mater* **2005**, *15*, 2005-2010, https://doi.org/10.1002/adfm.200500274.

Supplementary materials

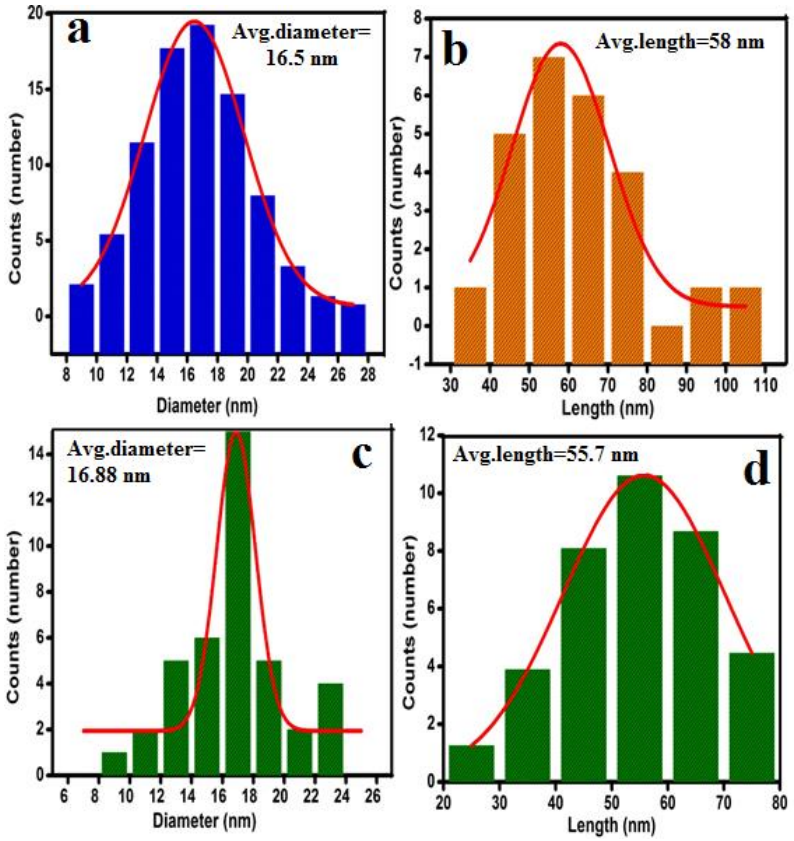

Figure S1. (a,b) histogram of diameter and length size distribution of HAp NRs_{sol12}, and (c,d) histogram of diameter and length size distribution of HAp NRs_{sol24}.

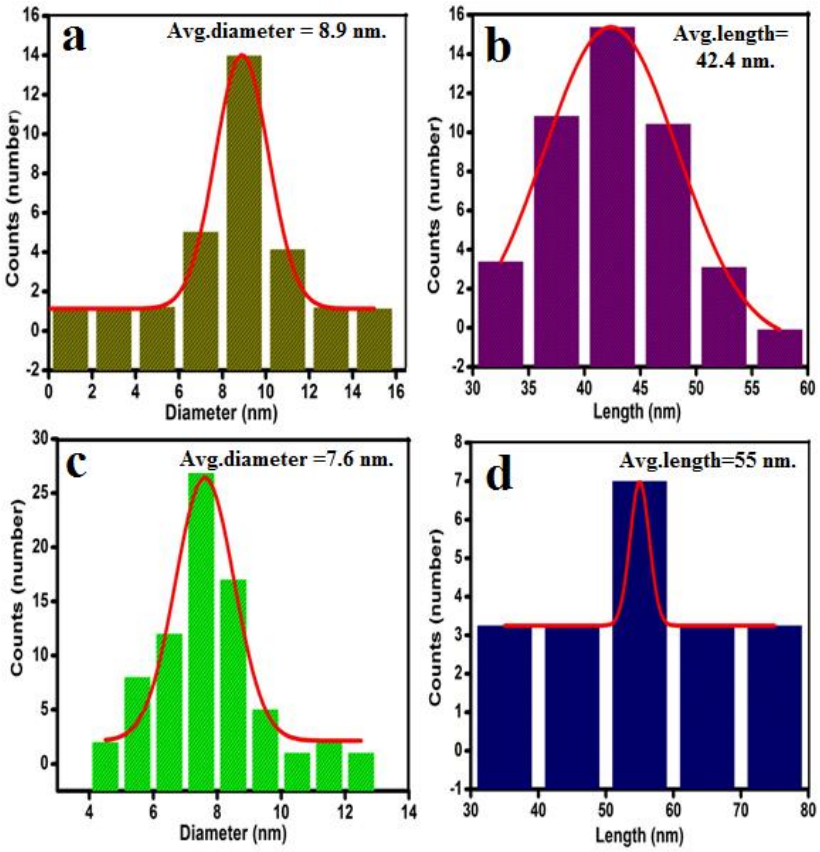

Figure S2. (a,b) histogram of diameter and length size distribution of HAp NRs_{MW10}, and (c,d) histogram of diameter and length size distribution of HAp NRs_{MW30}.

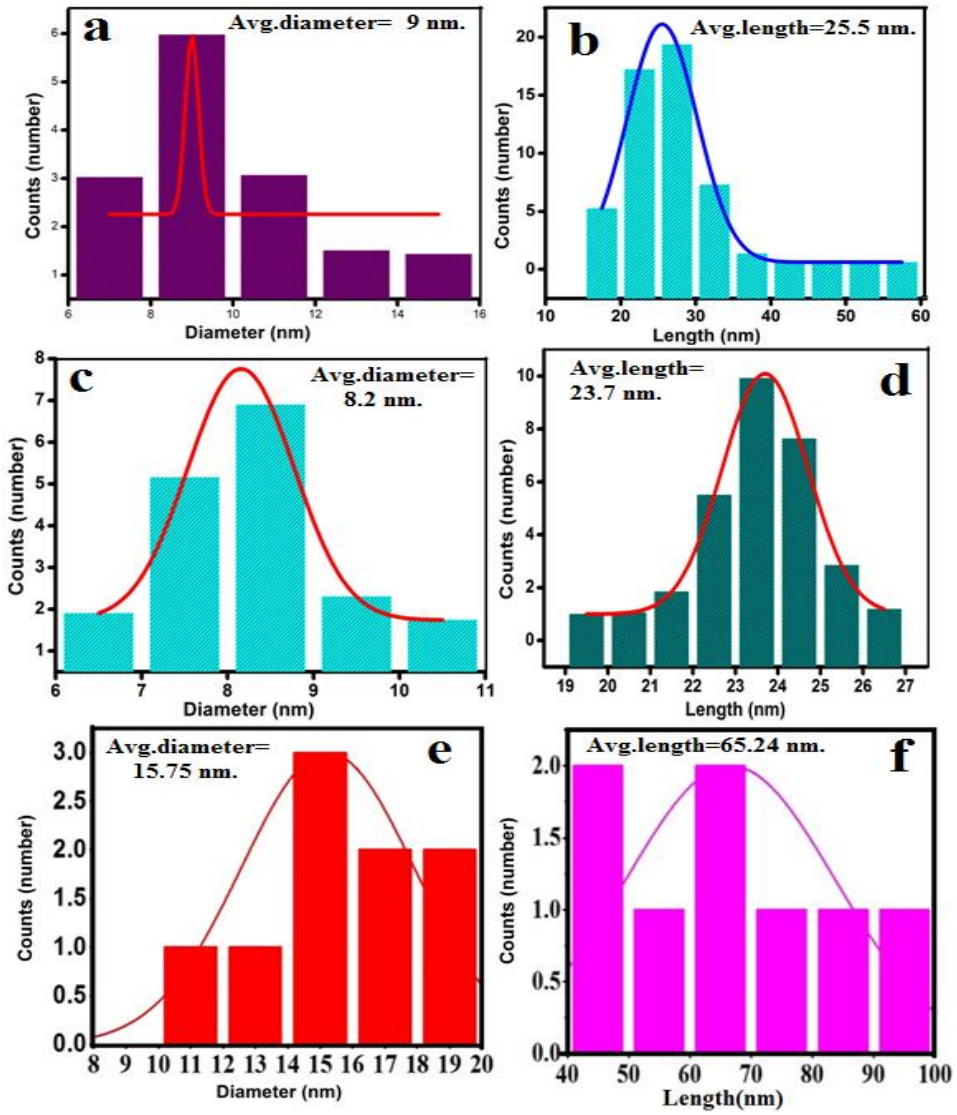

Figure S3. (a,b) histogram of diameter and length size distribution of HAp NRs_{ppt}, (c,d) histogram of diameter and length size distribution of CF-HAp NRs_{ppt}, and (e,f) histogram of diameter and length size distribution of CF-HAp $NRs_{hyd.}$